Strong Spin-Orbit Interaction Induced by Transition Metal Oxides at the Surface of Hydrogen-Terminated Diamond

Kaijian Xing [a], Daniel L. Creedon [b], Steve A. Yianni [a], Golrokh Akhgar [c, d], Lei Zhang [e], Lothar Ley [a, f], Jeffrey C. McCallum [b], Dongchen Qi *[, a, g], Christopher I. Pakes *[, a]

[a] *Department of Chemistry and Physics, La Trobe Institute for Molecular Science, La Trobe University, Bundoora, Victoria 3086, Australia*

[b] *School of Physics, The University of Melbourne, Victoria 3010, Australia*

[c] *ARC Centre of Excellence in Future Low-Energy Electronics Technologies, School of Physics, Monash University, Clayton, Victoria 3800, Australia*

[d] *School of Science, RMIT University, Melbourne, Victoria 3001, Australia*

[e] *Department of Physics, National University of Singapore, 2 Science Drive 3, Singapore 117542, Singapore*

[f] *Institute for Condensed Matter Physics, Universität Erlangen, Staudt-Str. 1, 91058 Erlangen, Germany*

[g] *School of Chemistry, Physics and Mechanical Engineering, Queensland University of Technology, Brisbane, Queensland 4001, Australia*

Abstract:

Hydrogen-terminated diamond possesses an intriguing *p*-type surface conductivity which is induced via thermodynamically driven electron transfer from the diamond surface into surface acceptors such as atmospheric adsorbates, a process called surface transfer doping. High electron affinity transition metal oxides (TMOs) including MoO_3 and V_2O_5 have been shown to be highly effective solid-state surface acceptors for diamond, giving rise to a sub-surface two-dimensional (2D) hole layer with metallic conduction. In this work, low temperature magnetotransport is used as a tool to show the presence of a Rashba-type spin-orbit interaction with a high spin-orbit coupling of 19.9

meV for MoO_3 doping and 22.9 meV for V_2O_5 doping, respectively, through the observation of a transition in the phase-coherent backscattering transport from weak localisation to weak antilocalization at low temperature. Surface transfer doping of diamond with TMOs provides a 2D hole system with spin-orbit coupling that is over two times larger than that reported for diamond surfaces with atmospheric acceptors, opening up possibilities to study and engineer spin transport in a carbon material system.

1. Introduction

Despite being a bona fide wide bandgap insulator, hydrogen-terminated diamond, once exposed to moist air, develops a *p*-type surface conductivity. The underlying mechanism, known as surface transfer doping, induces a spontaneous sub-surface, quasi-two-dimensional (2D) hole accumulation layer with an areal density of typically 10^{13} cm^{-2} without the need to introduce impurities into the diamond lattice [1, 2]. This simple yet effective doping scheme overcomes the limitation caused by conventional bulk doping (e.g. by boron substitution) [3], such as high dopant activation energy and carrier freeze-out at low temperature, and also offers a platform for the exploration of quantum transport phenomena in the resulting 2D hole gas (2DHG) at low temperature. Recent improvements in diamond bulk and surface quality have permitted hydrogen-terminated samples to be fabricated which support metallic conduction in the surface to sub-K temperatures [4]. This has allowed the observation of a surprisingly strong spin-orbit interaction in the diamond 2DHG with a measured spin-orbit splitting of 9.74 ± 0.1 meV [5] manifested in the form of phase-coherent quantum transport effects. Using an ionic-liquid gating approach, the spin-orbit splitting energy can be tuned over a wide range from 4.6 meV to 24.5 meV, opening up possibilities for the study of spin-coherent transport in diamond and the development of

*Corresponding authors: c.pakes@latrobe.edu.au; dongchen.qi@qut.edu.au

spintronic devices such as a spin field-effect transistor [6]. As reported previously, the spin-orbit interaction strength increases with the carrier concentration of the 2D hole band *via* the Rashba effect [6] induced by the highly asymmetrical surface confining potential as a result of surface transfer doping. Therefore, a higher hole density is expected to yield an even stronger spin-orbit interaction and permit an even wider dynamic range of spin-orbit coupling to be achieved. In recent years, there have been extensive reports demonstrating that high electron affinity transition metal oxides (TMOs), such as Nb_2O_5 [7], ReO_3 [8], WO_3 [7, 8], MoO_3 [9, 10], and V_2O_5 [7, 11], act as excellent surface acceptors which can induce hole density in the range of 1.8×10^{13} cm^{-2} to 2.5×10^{14} cm^{-2} on hydrogen-terminated diamond surfaces, comparable or higher than that achievable by air-induced doping. Furthermore, the TMO-induced hole accumulation layer exhibits improved thermal stability and operational stability compared to the air-induced surface conductivity [12]. However, the low-temperature phase-coherent quantum transport in the 2DHG on diamond induced by TMOs transfer doping has so far not been explored.

In this study, we use low-temperature magnetotranport as a tool to probe the phase-coherent transport in the 2D hole layer on hydrogen-terminated diamond induced by surface transfer doping with the two representative TMOs, i.e. MoO_3 and V_2O_5, and quantitatively analyze the spin-orbit interaction in this system by fitting to 2D localization theory. Through transfer doping with TMOs, a very strong spin-orbit coupling is achieved: 19.9 ± 2 meV for the MoO_3-hydrogen-terminated-diamond interface and 22.9 ± 2 meV for the V_2O_5-hydrogen-terminated-diamond interface. These are over two times larger than the previously reported value for ungated air-induced surface conducting diamond (9.74 ± 0.1 meV) [5].

2. Experimental

Hall bar devices were fabricated using commercial (Element Six) type-IIa 100-orientated single-crystal diamond substrates. Hydrogen-termination was carried out via exposure to a microwave hydrogen plasma, operating at a power of 1700 W, with a sample temperature of 850 °C for 10 minutes. Hall bar devices were subsequently fabricated using standard photolithography techniques. The active Hall bar regions (Fig.1) were defined and isolated by exposing the surrounding regions of the sample to a 50 W room-temperature oxygen plasma. Palladium contacts (100 nm) were formed by deposition using an electron-beam evaporator forming metal-diamond contacts displaying Ohmic behaviour at low temperature. [APL 116 111601 2020] Following fabrication of the diamond Hall bars, the sample was annealed to a temperature of 400 °C for 30 minutes in an ultra-high vacuum (UHV) system with a base pressure of 7×10^{-10} mbar to completely remove adsorbed water and atmospheric adsorbates while keeping the hydrogen-termination intact. In the same vacuum, MoO_3 (Device A) and V_2O_5 (Device B) were thermally deposited via a standard Knudsen cell (Fermion Instrument) onto the active region of the Hall bars through a precisely-aligned shadow mask as shown in Fig.1(c).

Magnetotransport measurements were carried out over the temperature range from 0.25 K to 20 K using a Leiden Cryogenics dry dilution refrigerator with a 9-1-1 T superconducting vector magnet. Standard AC lock-in measurements were employed to record simultaneously the longitudinal voltage V_{xx} and Hall voltage V_{xy} (Fig.1(a)) from which the corresponding symmetrised resistivities ρ_{xx} and ρ_{xy} were determined as a function of temperature and magnetic field applied perpendicular to the sample surface.

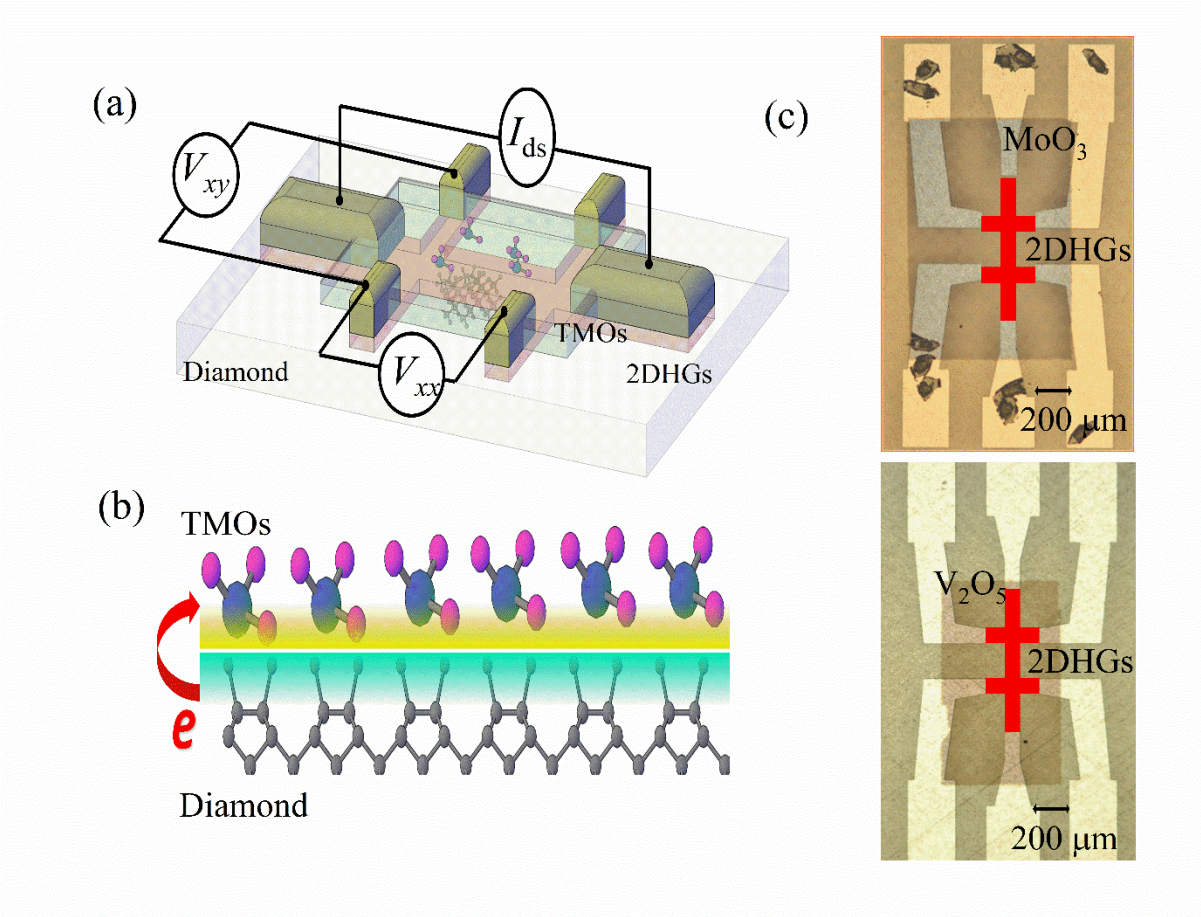

Fig. 1. (a) Configuration of TMO (MoO_3, V_2O_5) doped Hall bar devices; (b) cross section of the TMO/hydrogen-terminated-diamond interface with electron exchange (c) Optical image of TMO (MoO_3, V_2O_5) doped Hall bar device; the grey rectangle is the TMO layer deposited through a shadow mask after annealing in ultra-high vacuum (see text).

3. Results and discussion

The zero-field conductivity, $\sigma_{xx}(B = 0\ \mathrm{T})$, displays a weakly temperature-dependent behavior in both TMO-doped devices rather than an exponential dependence observed in previous work [13, 14], which rules out the carrier freeze-out and demonstrates a metallic conductivity at the hydrogen-terminated diamond surface introduced by TMO surface transfer doping. As shown in Fig.2, $\sigma_{xx}(B = 0\ \mathrm{T})$ has a logarithmic relationship with temperature similar to that observed for air-induced surface conducting diamond devices [5, 6], which demonstrates that the TMO-induced surface conductivity manifests a hole accumulation layer with Fermi liquid nature [15]. The weakly temperature-dependent conductivity observed in both devices is due to quantum corrections to the Drude conductivity that are characteristic of two-dimensional electronic systems: the hole-hole interaction (HHI) and phase coherent backscattering in the form of weak localization (WL) and weak antilocalization (WAL). HHI and phase coherence backscattering cause a similar logarithmic correction to the Drude conductivity at low temperature. A significant difference between these two corrections is that the HHI impacts both the Hall and longitudinal resistivities but is independent of magnetic field, whereas phase coherence backscattering plays no role in the Hall resistivity but introduces a distinctive signature to the longitudinal resistivity versus magnetic field curves through quantum interference corrections. This makes it possible to isolate the HHI contribution and independently probe the WL and WAL effects in the 2D hole layer [15, 16].

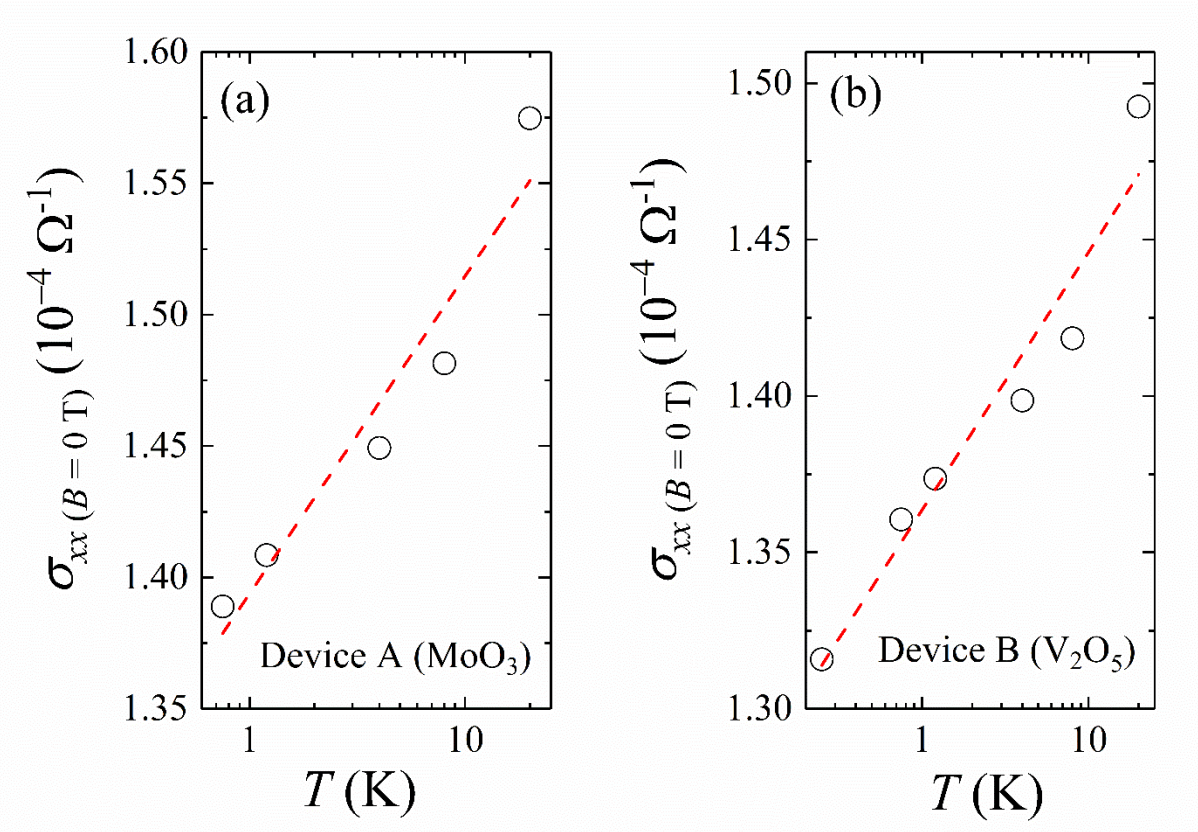

Fig. 2. Temperature dependence of the zero-field conductivity σ_{xx}(B = 0 T), illustrating logarithmic temperature dependence for (a) MoO_3 and (b) V_2O_5 doped devices.

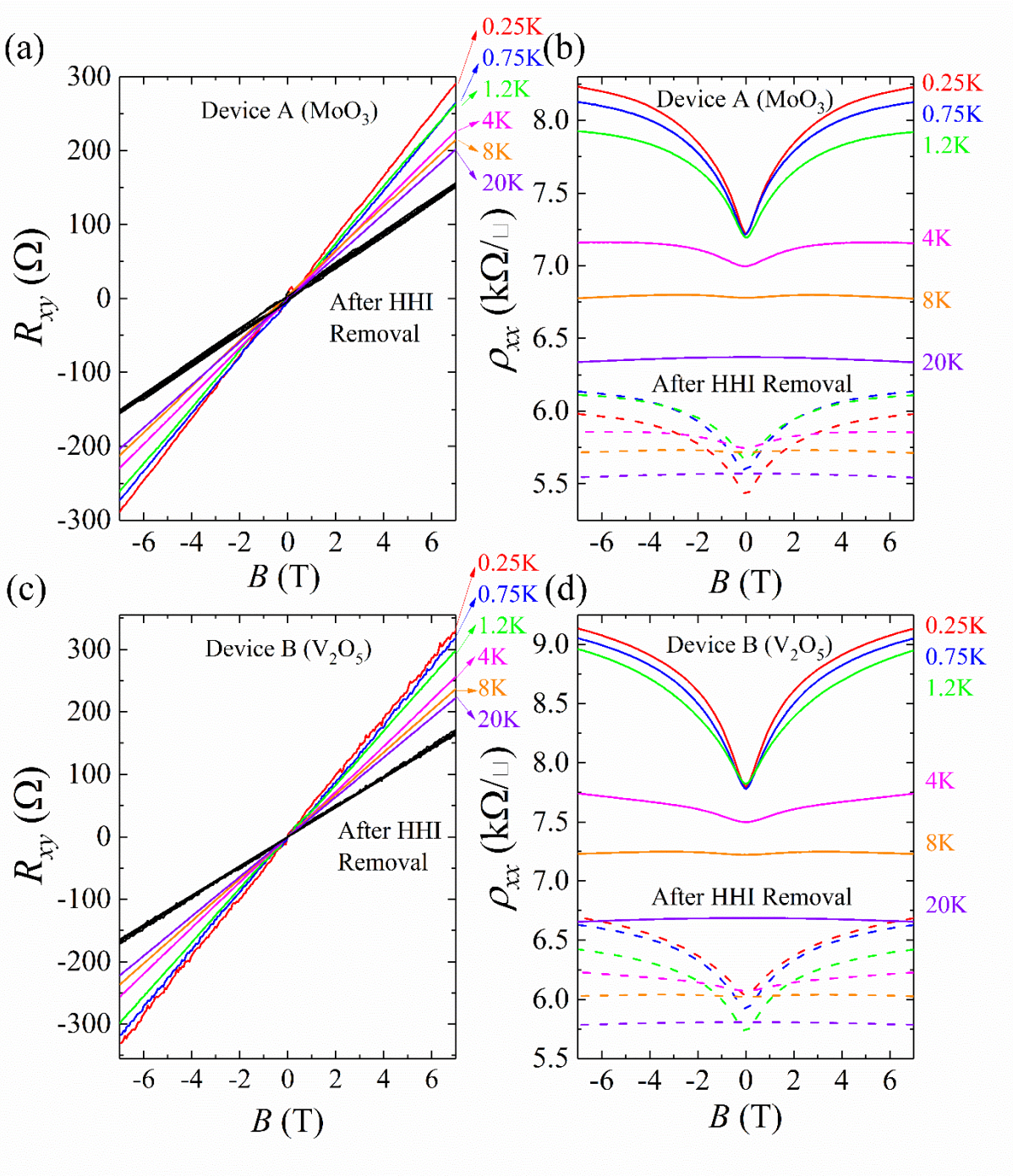

Fig. 3. Original $R_{xy}(B)$ data for TMOs-doped devices at different temperatures and the corrected R_{xy}(B) data after HHI removal (all cureves collapsed onto on signle black trace) for: (a) Device A (MoO_3), (c) Device B (V_2O_5). Original ρ_{xx}(B) for TMOs-doped devices at different temperatures and the corrected (dash lines) ρ_{xx}(B) after HHI removal for: (b) Device A (MoO_3), (d) Device B (V_2O_5).

As the phase coherent backscattering does not impact Hall resistance, all $\rho_{xy}(B)$ curves should collapse onto one single trace regardless of temerpature after removal of the HHI. The temperature-dependent correction to the Drude conductivity arising from the HHI takes the form [15]:

$$\Delta\sigma_{HH} = K_{HH} G_0 \ln\left(\frac{kT\tau_{tr}}{\hbar}\right) \qquad \text{Eq.}(1),$$

where $G_0 = e^2/\pi h$, K_{HH} is the interaction strength, and τ_{tr} is the transport relaxation time. The accurate determination of K_{HH} is required to account for the HHI correction. Following the approach of Goh *et.al.* [15], and also used by Edmonds *et.al.* [5] and Akhgar *et.al.* [6], an initial value for K_{HH} can be calculated directly from the slope of ΔR_H vs. $\ln\left(T / T_{reference}\right)$; see Fig.S1 in the Supplementary Information (SI). The value of K_{HH} is then systematically adjusted until all $\rho_{xy}(B)$ curves collapse onto one single, termperature-independnet trace as shown in Fig.3(a) and Fig.3(c). The final value of K_{HH} was found to be 0.429 ± 0.002 for Device A (MoO_3) and 0.437 ± 0.002 for Device B (V_2O_5), which is comparable to the value found for air-induced surface conducting diamond [5, 6]. After HHI removal, corrected hole carrier concentrations were derived from the slope of $\rho_{xy}(B)$, giving 2.84×10^{13} cm^{-2} for Device A and 2.69×10^{13} cm^{-2} for Device B. We note that the hole densities recorded in these devices are considerably smaller than achieved densities for TMO-doped diamond reported in the literature [7, 10] and we will return to this point later.

Fig.3(b) and Fig.3(d) depict both original (solid lines) and HHI-corrected (dashed lines) $\rho_{xx}(B)$ curves for the MoO_3 and V_2O_5 transfer doped Hall bars respectively. The pronounced features in the magnetoresistance around zero magnetic field are characteristic of the quantum interfernce effects in the form of WL and WAL in 2D electronic systems. At 20 K a negative magnetoresistance around B = 0 T arises from WL (Fig.S2), while a clear positive

magnetoresistance cusp, caused by WAL, can be observed in the data recorded at 8 K and below (Fig.S2). The intensity of the WAL cusps become stronger as the temperature decreases, indicating that the the spin-relaxiation driven WAL becomes the dominant quantum mechanical interference mechanism at low temperature. These observations are consisent with previous work that has used phase coherent scattering to probe the spin transport properties in the hydrogen-terminated diamond devices with an air-induced surface conductivity [5, 6]; we therefore follow the same approach to model the magnetoconductance in order to evaluate the spin-orbit interaction in TMO doped surfaces. It is worth noting that the corrected $\rho_{xx}(B)$ curves (dashed lines in Fig.3(b) and Fig.3(d) at different temperatures do not collapse onto a single value of the sheet resistivity value at ± 7 T because of a high characteristic transport field (B_{tr} = 27.4 T for MoO_3, B_{tr} = 28.2 T for V_2O_5), so that the applied magnetic fields in this case are not strong enough to completely suppress the WL effect. Here B_{tr} can be calculated by $B_{tr} = \hbar / \left(4eD\tau_{tr}\right)$, in which D and τ_{tr} is the diffusion constant and transport relaxation time, respectively.

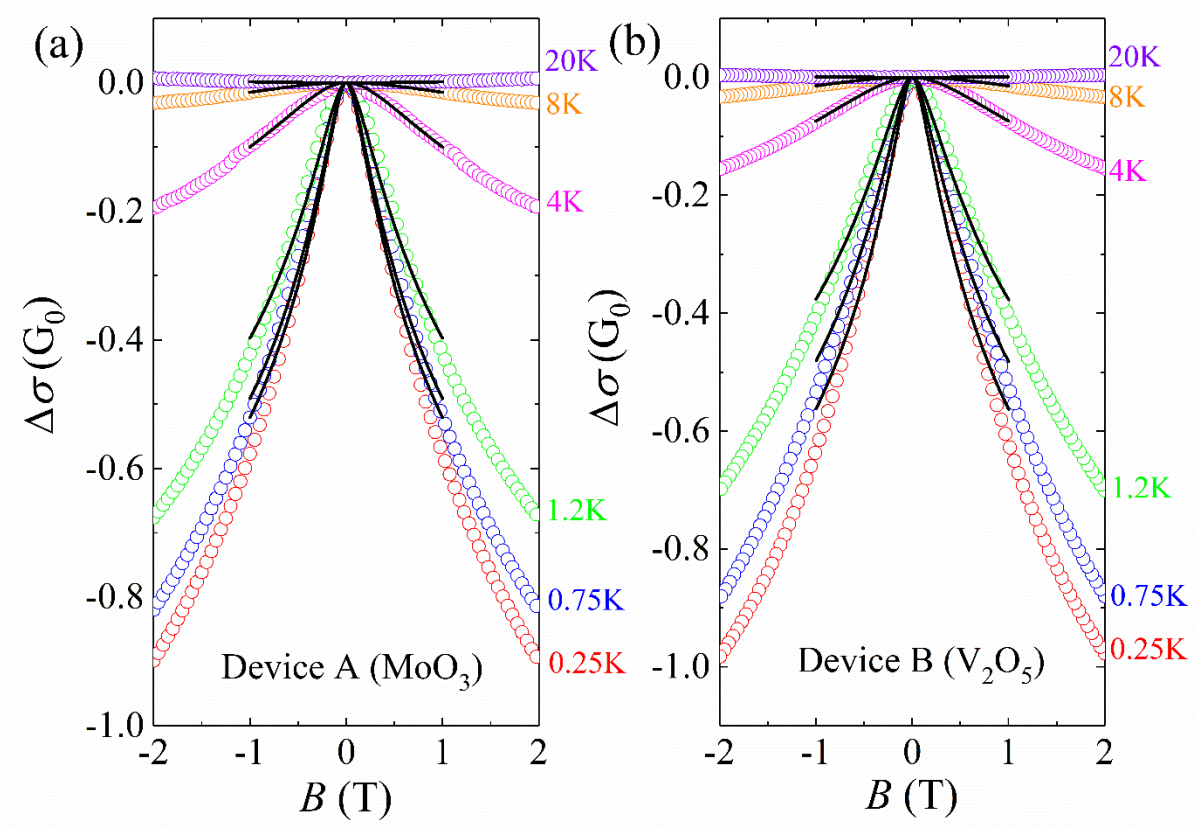

Fig. 4. Reduced magnetoconductivity in units of $G_0 = e^2/\pi h$ at different temperature: (a) Device A (MoO_3); (b) Device B (V_2O_5). The open circles represent the experimental data, and the solid lines are fits to theory.

WAL arises when a material experiences strong spin-orbit interaction and is typically seen in 2D electronic systems in which the spin-orbit coupling is further enhanced by the reduced dimension. The spin-orbit interaction exists only in crystals without inversion symmetry, which could arise either from a bulk inversion asymmetry (Dresselhaus effect) or an induced asymmetry (Rashba effect) through an engineered asymmetric confinement potential. In hydrogen-terminated diamond the WAL may arise from either anisotropy of the crystal, due to the hydrogen termination and (2 × 1) surface reconstruction, or from asymmetry of the 2D surface confining potential that leads to the surface hole accumulation. Previous work has shown that the theoretical models for Dresselhaus and Rashba driven WAL both fit experimental data well and give similar values of experimental parameters [5]. However, our

previous work in air-induced conducting devices showing that the spin-orbit coupling can be tuned over a wide range with an electrostatic gate suggests that the Rashba effect is the dominant mechanism [6]. In addition, the heavy hole nature of surface conducting diamond has been reported in literatures [17, 18], suggesting a k^3 Rashba interaction rather than a k-linear Rashba interaction. We therefore use the 2D localization theory described by Bergmann and Hikami [14, 16], appropriate for a k^3 Rashba interaction in a 2D hole system, to describe the observed changes in magnetoconductivity caused by WL and WAL in the current case:

$$\frac{\Delta\sigma}{G_0} = -\left\{ \begin{array}{l} \psi\left(\frac{1}{2}+\frac{B_\phi + B_{SO}}{B}\right) + \frac{1}{2}\cdot\psi\left(\frac{1}{2}+\frac{B_\phi + 2\cdot B_{SO}}{B}\right) - \frac{1}{2}\cdot\psi\left(\frac{1}{2}+\frac{B_\phi}{B}\right) \\ -\ln\left(\frac{B_\phi + B_{SO}}{B}\right) - \frac{1}{2}\cdot\ln\left(\frac{B_\phi + 2\cdot B_{SO}}{B}\right) + \frac{1}{2}\cdot\ln\left(\frac{B_\phi}{B}\right) \end{array} \right\} \qquad \text{Eq.}(2),$$

where ψ is the digamma function. The characteristic phase- and spin- field are B_ϕ and B_{SO}, which can be defined by $B_\phi = \hbar/\left(4eD\tau_\phi\right)$ and $B_{SO} = \hbar/\left(4eD\tau_{SO}\right)$, respectively. Here, τ_ϕ is the phase coherence time, τ_{SO} is the spin coherence time.

In order to compare and model the magnetoconductivity data for different temperatures, we plot in Fig.4 the change in low field magnetoconductivity $\Delta\sigma = \sigma(B) - \sigma(B=0)$ in the unit of $G_0 = e^2/\pi h$. The open circles represent the experimental data at different temperatures, i.e. 20 K (purple), 8 K (orange), 4 K (pink), 1.2 K (green), 0.75 K (blue) and 0.25 K (red). The black lines in Fig.4 correspond to a least-square fit of the experimental data using equation (2) and good agreement with the experimental data is observed at all temperatures within the diffusive regime ($B << B_{tr}$) [19, 20]. The single theoretical model describes well the transition from WL to WAL as the temperature decreases. The magnetoconductivity is positive,

corresponding to WL effect, at 20 K for both MoO_3 and V_2O_5 doped devices. At 8 K and below a negative magnetoconductivity develops close to zero field which grows with decreasing temperature.

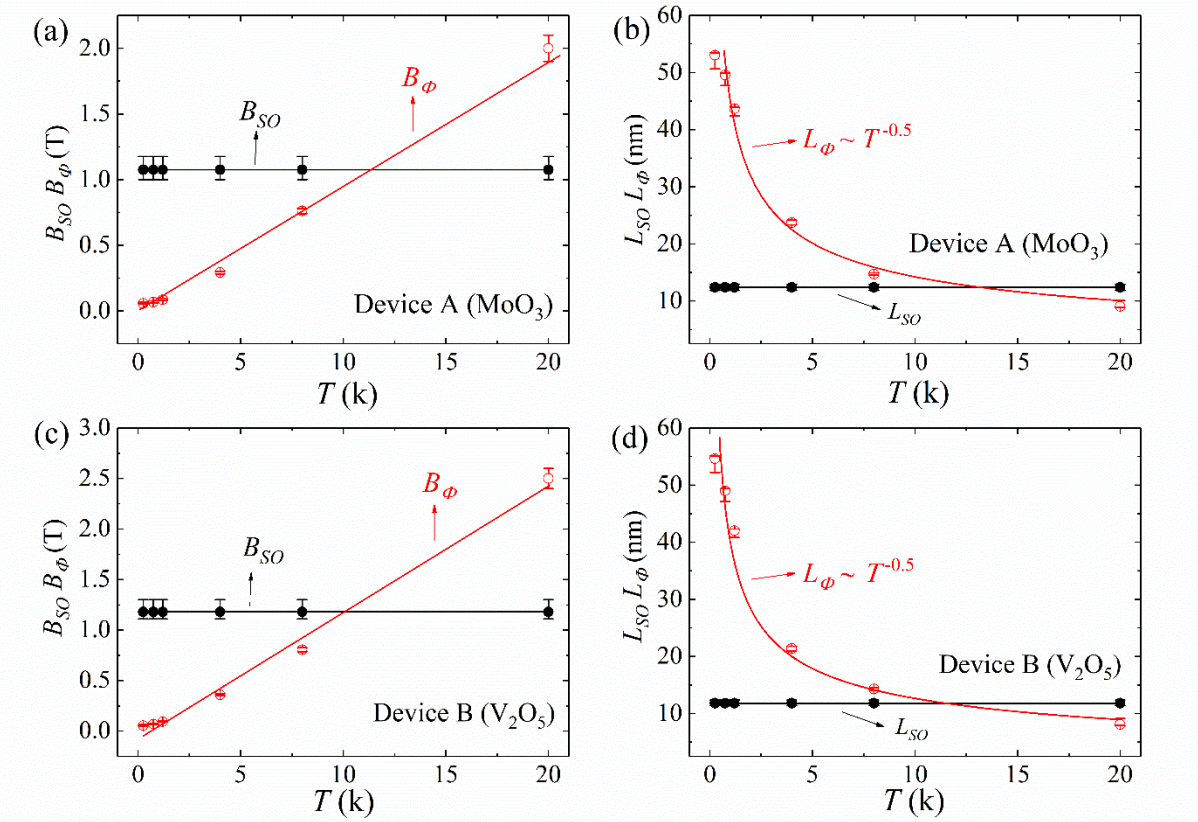

Fig. 5. Temperature dependence of the characteristic spin coherence field B_{SO} (solid black circles) and phase coherence field B_ϕ (open red circles): (a)Device A (MoO_3); (c) Device B (V_2O_5). The lines are linear fits to the data. Temperature dependence of the characteristic spin coherence length L_{SO} (solid black circles) and phase coherence length L_ϕ (open red circles): (b) Device A (MoO_3); (d) Device B (V_2O_5). The black lines are linear fits to L_{SO}. The red curves are $T^{-0.5}$ fit to L_ϕ.

As reported in previous work [5, 6], the ratio of the phase-coherence rate (τ_ϕ) and the spin-relaxation rate (τ_{SO}) governs the evolution from WL to WAL. As $B_\phi = \hbar / \left(4eD\tau_\phi\right)$ and

$B_{SO} = \hbar / \left(4eD\tau_{SO}\right)$, the key ratio can be simply converted to B_{SO}/B_{ϕ}. By fitting the magnetoconductivity data, these important fitting parameters can be extracted and are plotted as a function of temperature in Fig.5 (a) for Sample A (MoO_3); Fig.5(c) for Sample B (V_2O_5). B_{SO} is temperature independent as expected in a degenerate system with charge transport dominated by carriers near the Fermi surface [5, 6]. In contrast, B_{ϕ} increases almost linearly with the temperature due to the Nyquist dephasing [21]. Following evaluation of B_{SO} and B_{ϕ}, the corresponding phase and spin coherence lengths can be calculated according to $L_{\phi} = \left[\hbar / \left(4eB_{\phi}\right)\right]^{0.5}$ and $L_{SO} = \left[\hbar / \left(4eB_{SO}\right)\right]^{0.5}$ as illustrated in Fig.5 (b) and Fig.5 (d). For both MoO_3 and V_2O_5 doped devices, L_{ϕ} is found to be proportional to $T^{-0.5}$, giving clear evidence of the 2D nature of the hole layer induced by TMO doping [5]. For both devices a spin coherence length, L_{SO}, of approxmiate 12 nm is determined, which is appropriate given the similar hole densities achieved using the two TMOs. The relative size of L_{SO} and L_{ϕ} conveniently describes the transition from WL to WAL. In a system with strong spin-orbit interaction the spin of a carrier is coupled to its momentum. At low temperature where spin-coherence length L_{SO} is shorter than the phase coherence length L_{ϕ}, backscattering loops are sufficiently large such that spin coherence is lost and the spin rotates as it goes around time-reversed self-intersection paths, leading to destruction interference with characteristic WAL cusp in the magnetoconductivity at low magnetic field. At high temperature for which $L_{\phi} < L_{SO}$, spin coherence is maintained over the entire backscattering loop and the time-reversed, self-intersecting path interferes constructively similar to that of spinless particles, consequently the phase-coherent transport is dominated by WL with positive magnetoconductivity. The crossing points in Fig.5(a) to Fig.5(d) qualitatively reflect the transition temperature.

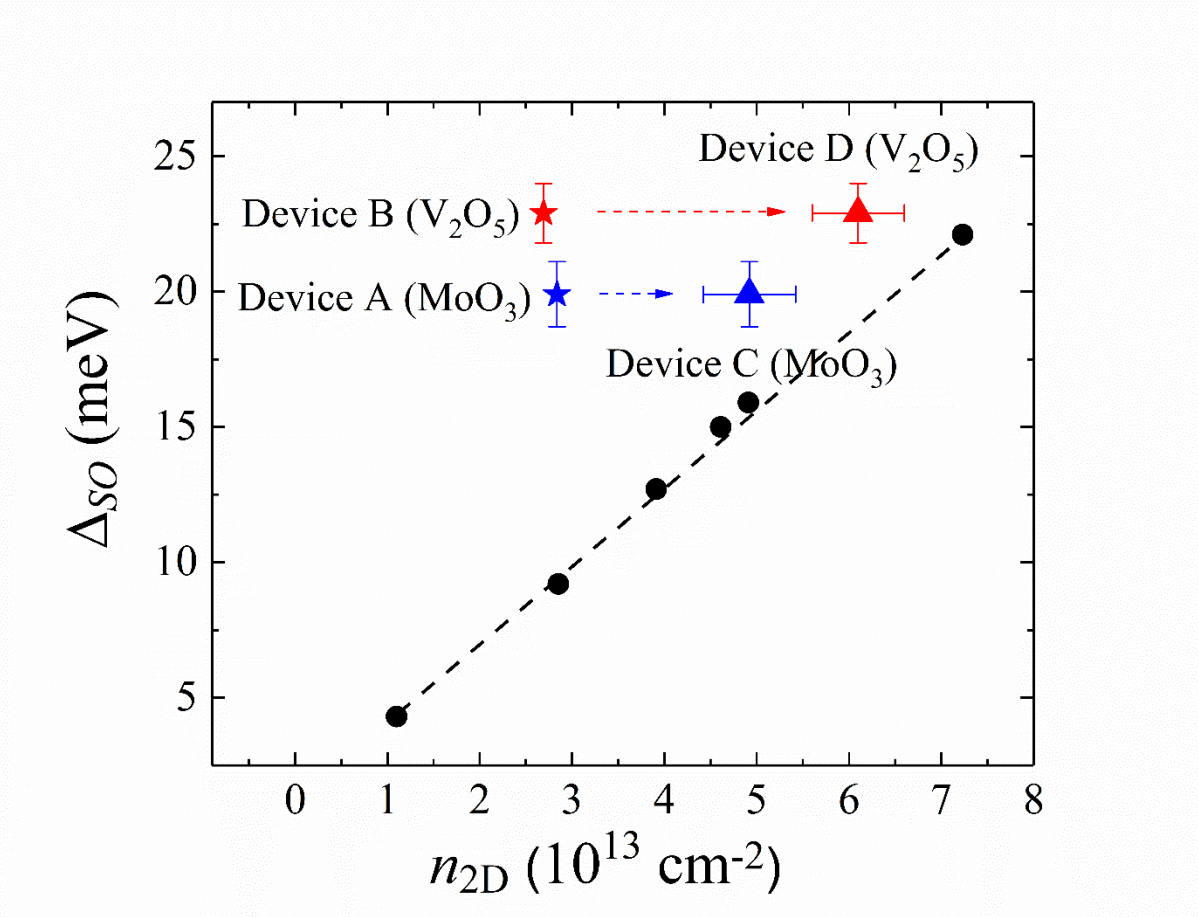

Fig. 6. Spin-orbit interaction strength (Δ_{SO}) plotted as a function of hole density. The solid stars represent measurements from Hall bar devices (A and B); the solid triangles represent the same Δ_{SO} values but with the hole density adjusted to the value determined for the corresponding Van der Pauw devices (C and D).The solid circles are spin-orbit interaction data for air-induced surface conducting devices taken from Ref. 6.

Having quantified the WL and WAL from the experimental magnetoconductivity curves, we now turn to the evaluation of the spin-orbit interaction strength , Δ_{SO}, which is related to the spin relaxation time (τ_{SO}) and transport relaxation time (τ_{tr}), as given by $\tau_{SO} = \hbar/\left(4eDB_{SO}\right)$ and $\tau_{tr} = \hbar/\left(4eDB_{tr}\right)$. The corresponding Δ_{SO} are 19.9 ± 2 meV for Device A (MoO_3) and 22.9 ± 2 meV for Device B (V_2O_5) hydrogen-terminated-diamond interface, which is calculated by

$\Delta_{SO} = \hbar / \left(2\tau_{tr}\tau_{SO}\right)^{0.5}$ [5, 6]. In both cases, the spin-orbit interaction strength is found to be at least two times higher than the value of 9.74 meV determined for the air-induced surface conducting diamond devices [5]. Hence we demonstrate that a strong Rashba spin-orbit interaction can be induced by doping the hydrogen-terminated diamond surface with TMOs.

As noted earlier, the achievable spin-orbit coupling, as a result of the Rashba effect, should be dependent on the asymmetry of the quantum well that confines the carriers to a 2D sheet which in turn is related to the charge carrier density via the Poisson equation. In principle Δ_{SO} should increase with increasing n_{2D} for Rashba effect. Indeed, previous work on air-induced surface conducting devices and devices gated with ionic liquid has shown that Δ_{SO} increases proportionally to the hole density [6]. It is therefore interesting to see if the spin-orbit splitting derived above for TMO-induced 2D conducting channel is consistent with a universal relationship between Δ_{SO} and n_{2D} derived from the air-induced, ionic-liquid gated devices [6]. In Fig.6, the spin-orbit interaction energies for both for both Device A (MoO_3) and Device B (V_2O_5) are plotted alongside previous data from ref. [6]. Intriguingly, the spin-orbit coupling strengths in the TMO-induced 2D hole layer are significantly larger than those at similar hole densities achieved with electrostatic gating. In another word, to account for the high Δ_{SO} in the present case, higher hole densities are expected in the TMO transfer doped channel to appear consistent with the universal relationship. We argue that this discrepancy can be explained by a spatial inhomogeneity of the hole density in the diamond surface conducting channel which has been reported elsewhere with a fluctuation as large as an order of magnitude both for air-induced as well as gated surface conducting devices [22~24]. The spin-orbit interaction is a localised effect which occurs on the sub-100 nm length scale characterised by the phase and spin coherence lengths and is probed through the WAL correction to the conductivity. In contrast, the hole density derived from Hall effect measurements is based upon a macroscopic

measurement of the device as a whole. Consequently, the local carrier density on diamond, giving rise to the high spin-orbit interaction strength as dictated by WAL, could be much higher than the macroscopically averaged hole density derived from Hall effect measurements. In addition, there are several mechanisms that could contribute to the laterally inhomogeneous hole carrier distribution in the surface conducting channel. For example, a spatial inhomogeneity of the diamond surface or of the TMO layer might cause local fluctuation in the density of surface acceptors, and hence the induced hole density. As noted earlier the hole densities in the present diamond Hall bar devices are considerably lower than hole densities reported elsewhere [7, 10]. In the latter cases, TMOs were deposited directly onto pristine surfaces of hydrogen-terminated diamond without any further device fabrication. This suggests that photoresist residues as a result of the device fabrication process [25] could also potentially affect the local hole density by interfering with the surface transfer doping process between diamond and TMOs. In order to test this hypothesis Hall effect measurements were performed on two additional hydrogen-terminated diamond samples in a simple Van der Pauw (VdP) geometry with conductive epoxy on the four corners of the samples. Both samples were subsequently annealed in UHV with subsequent *in-situ* TMO deposition, following the same approach described earlier. In this way, the surface of the hydrogen-terminated diamond samples can be kept as pristine as possible before exposure to TMOs without undergoing any photolithography processing. The hole densities for these two samples were determined as $(4.9 \pm 0.5) \times 10^{13}$ cm^{-2} when doped with MoO_3 (Device C) and $(6.1 \pm 0.5) \times 10^{13}$ cm^{-2} when doped with V_2O_5 (Device D). The VdP results are corrected to eliminate the overestimation of hole density compared with Hall bar results. [26] Both are indeed consistently higher than the hole density measured for the corresponding Hall bar devices, suggesting that the high spin-orbit interaction for MoO_3 and V_2O_5 induced 2D conducting layers is possibly derived from local regions of the surface in which the TMO-C (100):H interface is undisturbed and at which the

local hole density is approximate two times higher than the macroscopic hole density recorded for the device as a whole. The small drifting of the quantitatively corrected data points (solid triangles) from the universal line (Fig. 6) might arise from the systematically errors in the measurements, or be caused by the solid-state surface acceptors, which will be further studied in the future study.

4. Conclusions

In summary, we have shown that surface transfer doping by TMOs (MoO_3 and V_2O_5) at diamond surface produces a metallic two-dimensional hole layer with a strong spin-orbit interaction. The spin orbit interaction can be well described by the k^3 Rashba model, with a spin orbit coupling of 19.9 ± 2 meV for the MoO_3-hydrogen-terminated-diamond interface and 22.9 ± 2 meV for V_2O_5-hydrogen-terminated-diamond interface. These coupling strengths are significantly higher than that reported for air-induced surface conducting diamond [5], and other low-dimensional systems such as hydrogenated graphene [27], carbon nanotubes [28] and InAs quantum dots [29]~~, and this is explained by the local high hole density afforded by TMO transfer doping.~~ The reason, as noted above, is that the spin-orbit interaction arises through an asymmetry induced Rashba effect, which can be very large in diamond due to its ability to sustain a very high electric field, comparing with other materials. These results suggest that surface conducting diamond devices realised through TMO-based surface transfer doping provide a viable route to generate, control and convert spin currents, and has great potential for the study and development of all solid-state low-power spin transport devices.

Note

The author declare no competing financial interest.

Acknowledgments

This work was supported by the Australian Research Council under the Discovery Project (DP150101673) and Future Fellowship (FT60100207) schemes. This work was performed in part at the University of Sydney: Bandwidth Foundary International, part of the OptoFab node of the Australian National Fabrication Facilities.

Supplementary Information

There is another document specifically for the supplementary information

References

[1] F. Maier, M. Riedel, B. Mantel, J. Ristein, L. Ley, Origin of surface conductivity in diamond, Phys. Rev. Lett. 2000; 85(16): 3472–3475.

[2] Pakes, C. I.; Garrido, J. a.; Kawarada, H., Diamond Surface Conductivity: Properties, Devices, and Sensors, MRS Bull. 2014; 39: 542–548.

[3] R. Kalish, Diamond as a unique high-tech electronic material: difficulties and prospects, J. Phys. D. Appl. Phys. 2007; 40(20): 6467–6478.

[4] L. Ley, Preparation of low index single crystal diamond surfaces for surface science studies, Diam. Relat. Mater. 2011; 20(3): 418–427.

[5] M.T. Edmonds, L.H. Willems Van Beveren, O. Klochan, J. Cervenka, K. Ganesan, S. Prawer, L. Ley, A.R. Hamilton, C.I. Pakes, Spin-orbit interaction in a two-dimensional hole gas at the surface of hydrogenated diamond, Nano Lett. 2015; 15: 16–20.

[6] G. Akhgar, O. Klochan, L.H. Willems Van Beveren, M.T. Edmonds, F. Maier, B.J. Spencer, J.C. McCallum, L. Ley, A.R. Hamilton, C.I. Pakes, Strong and tunable spin-orbit coupling in a two-dimensional hole gas in ionic-liquid gated diamond devices, Nano Lett. 2016; 16: 3768–3773.

[7] C. Verona, W. Ciccognani, S. Colangeli, E. Limiti, M. Marinelli, G. Verona-Rinati, Comparative investigation of surface transfer doping of hydrogen terminated diamond by high electron affinity insulators, J. Appl. Phys. 2016; 120(2): 025104-1–7.

[8] M. Tordjman, K. Weinfeld, R. Kalish, Boosting surface charge-transfer doping efficiency and robustness of diamond with WO_3 and ReO_3, Appl. Phys. Lett. 2017;111 (11): 111601-1–5.

[9] S.A.O. Russell, L. Cao, D. Qi, A. Tallaire, K.G. Crawford, A.T.S. Wee, D.A.J. Moran, Surface transfer doping of diamond by MoO_3: A combined spectroscopic and Hall

measurement study, Appl. Phys. Lett. 2013; 103(20): 042103-1–4.

[10] M. Tordjman, C. Saguy, A. Bolker, R. Kalish, Superior Surface Transfer Doping of Diamond with MoO_3, Adv. Mater. Interfaces. 2014; 1(3): 1300155-1–6.

[11] K.G. Crawford, L. Cao, D. Qi, A. Tallaire, E. Limiti, C. Verona, A.T.S. Wee, D.A.J. Moran, Enhanced surface transfer doping of diamond by V_2O_5 with improved thermal stability, Appl. Phys. Lett. 2016; 108(4): 042103-1–4 .

[12] K.G. Crawford, D. Qi, J. McGlynn, T.G. Ivanov, P.B. Shah, J. Weil, A. Tallaire, A.Y. Ganin, D.A.J. Moran, Thermally Stable, High Performance Transfer Doping of Diamond using Transition Metal Oxides, Sci. Rep. 2018; 8: 3342-1–9.

[13] R. Winkler, Spin-orbit Coupling Effects in two-dimensional electron and hole systems, Springer-Verlag Berlin Heidelberg; 2003.

[14] S. Hikami, A.I. Larkin, Y. Nagaoka, Spin-Orbit Interaction and Magnetoresistance in the Two Dimensional Random System, Prog. Theor. Phys. 1980; 63(2): 707–710.

[15] K.E.J. Goh, M.Y. Simmons, A.R. Hamilton, Electron-electron interactions in highly disordered two-dimensional systems, Phys. Rev. B - Condens. Matter Mater. Phys. 2008; 77(23): 235410-1–9.

[16] G. Bergmann, WEAK LOCALIZATION IN THIN FILMS a time-of-flight experiment with conduction electrons, Phys. Rep. 1986: 3–58.

[17] H. Nakamura, T. Koga, T. Kimura, Experiental Evidence of Cubic Rashba Effect in an Inversion-Symmetric Oxide, Phys. Rev. Lett. 2012; 108: 206601-1–5.

[18] R. Moriya, K. Sawano, Y. Hoshi, S. Masubuchi, Y. Shirahi, A. Wild, C. Neumann, G. Abstreiter, D. Bougeard, T. Koga, T. Machida, Cubic Rashba Spin-Orbit Interaction of a Two-Dimensional Hole Gas in a Strained-Ge/SiGe Quantum well, Phys. Rev. Lett. 2014; 113 086601-1–5.

[19] M.I. Dyakonov, Magnetoconductance due to weak loalization beyong the diffusion approximation: the high-field limit, Solid State Commun. 1994; 92(8): 711–714

[20] A. Sawada, T. Koga, Universal modeling of weak antilocalizaition corrections in quasi-two-dimensional electron systems using predetermined return orbitals, Phys. REV. E 2017; 95: 023309-1–10.

[21] B.L. Altshuler, A.G. Aronov, D.E. Khmelnitsky, Effects of electron-electron collisions with small energy transfers on quantum localisation, J. Phys. C Solid State Phys. 1982; 15: 7367–7386.

[22] Y. Takahide, H. Okazaki, K. Deguchi, S. Uji, H. Takeya, Y. Takano, H. Tsuboi, H. Kawarada, Quantum oscillations of the two-dimensional hole gas at atomically flat diamond surfaces, Phys. Rev. B - Condens. Matter Mater. Phys. 2014; 89(23): 235304-1–5.

[23] G. Akhgar, D.L. Creedon, L.H. Willems Van Beveren, A. Stacey, D.I. Hoxley, J.C. McCallum, L. Ley, A.R. Hamilton, C.I. Pakes, G-factor and well width variations for the two-dimensional hole gas in surface conducting diamond, Appl. Phys. Lett. 2018; 112(4): 042102-1–5.

[24] G. Akhgar, L. Ley, D.L. Creedon, A. Stacey, J.C. McCallum, A.R. Hamilton, C.I.

Pakes, G -factor and well-width fluctuations as a function of carrier density in the two-dimensional hole accumulation layer of transfer-doped diamond, Phys. Rev. B. 2019; 99(3): 035159-1–6.

[25] D. Oing, M. Geller, A. Lorke, N. Wöhrl, Tunable carrier density and high mobility of two-dimensional hole gases on diamond: The role of oxygen adsorption and surface roughness, Diam. Relat. Mater. 2019; 97: 107450-1–5.

[26] R. Chwang, B. J. Smith, C. R. Crowell, Contact Size Effects on the Van Der Pauw Method for Resistivity and Hall Coefficient Measurement, Solid-State Electron 1974; 17: 1217–1227.

[27] J. Balakrishnan, G. Kok Wai Koon, M. Jaiswal, A.H. Castro Neto, B. Özyilmaz, Colossal enhancement of spin-orbit coupling in weakly hydrogenated graphene, Nat. Phys. 2013; 9: 284–287.

[28] G.A. Steele, F. Pei, E.A. Laird, J.M. Jol, H.B. Meerwaldt, L.P. Kouwenhoven, Large spin-orbit coupling in carbon nanotubes, Nat. Commun. 2013; 4: 1573-1–7.

[29] Y. Kanai, R.S. Deacon, S. Takahashi, A. Oiwa, K. Yoshida, K. Shibata, K. Hirakawa, Y. Tokura, S. Tarucha, Electrically tuned spin-orbit interaction in an InAs self-assembled quantum dot, Nat. Nanotechnol. 2011; 6: 511–516.